RSC Advances

PAPER

View Article Online
View Journal | View Issue

Cite this: *RSC Adv.*, 2026, **16**, 30111

Novel benzothiazole-indole acetamides as potential anticancer agents: synthesis, biological evaluation, and *in silico* studies

Nazanin Motamedi Shakib,†[a] Manica Negahdaripour, †[bc] Mohammad Hosein Sayahi,[d] Navid Dastyafteh,[e] Zahra Dehghani,[b] Mina Emami,[b] Sajedeh Safapoor,[f] Younes Ghasemi,[bc] Seyedeh Niloufar Ghafouri,[a] Abbas Ghahramani,[g] Mohammad Reza Mohajeri-Tehrani,[f] Bagher Larijani,[f] Mohammad Mahdavi*[f] and Sara Ranjbar *[b]

A series of novel benzothiazole-indole acetamides (**9a–n**) was designed and synthesized as potential anticancer agents, and their antiproliferative activities were evaluated against three cancer cell lines: A549 (human lung cancer), SW480 (human colon cancer), and HepG2 (human liver cancer). The most potent derivative identified was 2-(3-(benzo[*d*]thiazol-2-yl)-1*H*-indol-1-yl)-*N*-(2,4-dimethoxyphenyl) acetamide (**9d**) which demonstrated IC_{50} values of 7.9 ± 1.6, 16.1 ± 0.5, and 9.3 ± 2.2 μM against A549, SW480, and HepG2 cells, respectively, comparable or even superior to those of cisplatin (IC_{50}s were 5.7 ± 1.6, 15.2 ± 0.3, and 14.3 ± 1.9 μM for A549, SW480, and HepG2 cells, respectively). Notably, compound **9d** showed remarkably less toxicity on the normal MRC-5 than cisplatin. Cell cycle progression and apoptosis induction analyses revealed that **9d** arrested the cell cycle at G2/M phase and induced apoptosis in A549. *In silico* predictions regarding drug-likeness, pharmacokinetics, and toxicological characteristics suggest that the promising derivative **9d** could be proposed as a potential anticancer drug for further preclinical studies. Molecular docking studies revealed that **9d** was well accommodated within the endothelial growth factor receptor (EGFR) active site.

Received 28th October 2025
Accepted 24th May 2026

DOI: 10.1039/d5ra08263c

rsc.li/rsc-advances

1. Introduction

Cancer remains a leading global health concern, accounting for a significant proportion of deaths worldwide. In 2021, cancer was responsible for 14.5% of total deaths and 8.8% of total disability-adjusted life years (DALYs).[1] The global incidence of cancer continues to rise, with over 2 million new cases diagnosed in the United States alone in 2024.[2] Unfortunately, by 2030, the number of cancer-related deaths is expected to rise to approximately 13.1 million.[3]

Traditional cancer treatment modalities, including surgery, chemotherapy, and radiotherapy remain the cornerstone of cancer management. However, their limitations, including severe side effects, non-specific targeting, and tumor recurrence, necessitate the exploration of more advanced therapeutic approaches. Despite these advancements, the heterogeneity of tumor cells and their ability to develop resistance to treatment remain major obstacles.[4] These complexities necessitate the development of novel biologically active compounds and combination therapies that can improve patient outcomes; therefore, safer and more efficient compounds are needed.

Heterocyclic compounds represent a structurally diverse class of organic molecules characterized by the presence of at least one heteroatom—such as nitrogen, oxygen, or sulfur—incorporated within a cyclic ring system. These compounds are of significant importance in medicinal chemistry due to their broad spectrum of biological activities, including anticancer, antiviral, antibacterial, and anti-inflammatory effects.[5] Their distinct electronic properties render them highly valuable in various fields such as drug discovery, agrochemistry, and materials science.[5] The capacity of heterocyclic structures to engage in hydrogen bonding and other non-covalent

[a]*School of Chemistry, College of Science, University of Tehran, Tehran, Iran*
[b]*Pharmaceutical Sciences Research Center, Shiraz University of Medical Sciences, Shiraz, Iran. E-mail: ranjbar_sa@sums.ac.ir*
[c]*Department of Pharmaceutical Biotechnology, School of Pharmacy, Shiraz University of Medical Sciences, Iran*
[d]*Department of Chemistry, Payame Noor University, Tehran, Iran*
[e]*Center for Research of Endemic Parasites of Iran, Tehran University of Medical Sciences, Tehran, Iran*
[f]*Endocrinology and Metabolism Research Center, Endocrinology and Metabolism Clinical Sciences Institute, Tehran University of Medical Sciences, Tehran, Iran. E-mail: momahdavi@tums.ac.ir*
[g]*Department of Pharmaceutical Biotechnology, Faculty of Pharmacy, Kerman University of Medical Sciences, Kerman, Iran*
† These two authors contributed equally to this work, and both are considered as the first authors.

interactions with biological targets underpins their widespread use in pharmaceutical development, with over 85% of bioactive molecules featuring heterocyclic moieties.[5] Furthermore, the incorporation of heteroatoms modulates electron distribution, polarity, and hydrogen bonding capacity, thereby affecting the lipophilic characteristics of these compounds.[6]

Benzothiazole as a heterocyclic aromatic compound has recently gained considerable attention in the design and development of anticancer agents due to its unique structural and pharmacological properties. As a fused heterocyclic system comprising both benzene and thiazole rings, benzothiazole closely mimics the electronic distribution and steric configuration of the indole nucleus, thereby enabling enhanced molecular recognition and binding affinity to various biological targets implicated in cancer progression.[7,8] A simple benzothiazol derivative has been was extensively investigated as an anticancer agent (Fig. 1-I).[9] Riluzole (Fig. 1-II), a benzothiazole-containing medicine primarily used for amyotrophic lateral sclerosis (ALS), has shown potential anticancer effects. Recent studies indicate that riluzole can inhibit cancer cell proliferation and induce cell death in various cancer types, including skin, breast, pancreas, colon, liver, bone, brain, lung, and nasopharynx cancers. Riluzole shows antiproliferative activity against A549 cells with an IC_{50} value of 21.1 μM. It also induces apoptosis and arrests cell cycle G2/M in A549 cells.[10,11] The versatility of benzothiazole-based compounds in medicinal chemistry underscores their potential as effective anticancer

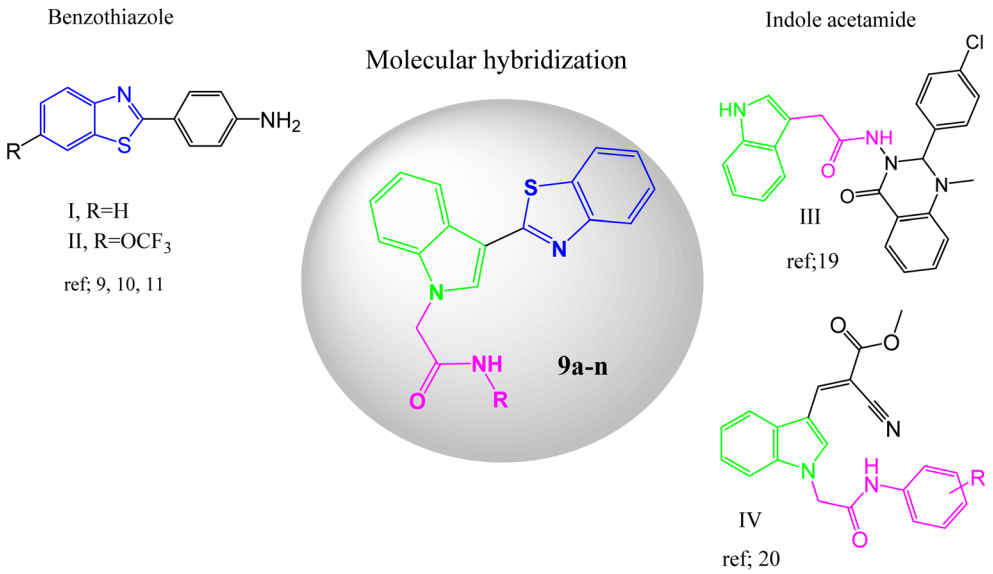

Fig. 1 Rationale design of the benzothiazole-indole acetamide hybrids (**9a–n**) as anticancer agents.

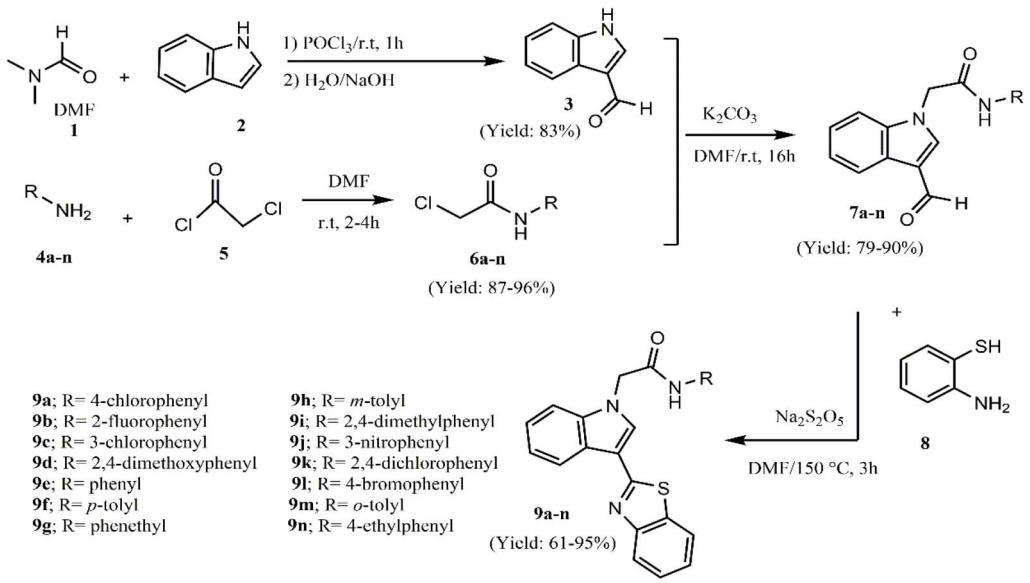

Scheme 1 Procedure for the synthesis of novel benzothiazole-indole-acetamides **9a–n**.

agents, warranting further investigation into their mechanisms and therapeutic applications.

Indole is also a prominent example of a heterocyclic aromatic compound, comprising a bicyclic structure formed by the fusion of a benzene ring with a pyrrole ring. This framework is regarded as a privileged scaffold in medicinal chemistry due to its frequent occurrence in pharmacologically active agents. The electron-rich aromatic system of indole facilitates robust interactions with biological macromolecules, enhancing both binding affinity and molecular selectivity. The nitrogen atom within the pyrrole ring contributes to the hydrogen bonding potential and influences the compound's lipophilicity, both of which are critical factors for cellular permeability and bioavailability.[12] Indole derivatives exhibit a wide array of therapeutic properties, including anticancer, antidiabetic, antimicrobial, anti-inflammatory, and antifungal activities, positioning them as key candidates in drug discovery efforts.[13] These compounds are characterized by favorable pharmacokinetic properties such as high bioavailability and low toxicity, along with strong affinities for a variety of biological targets, making them particularly attractive in the design of anticancer agents. Numerous studies have demonstrated that indole-based compounds can inhibit tumor proliferation, induce apoptosis, and modulate key signaling pathways implicated in cancer progression.[14] Many indole derivatives have been established as potent antitumor agents, including vinblastine, vincristine, eudistomin, sunitinib, osimertinib, and D-24851.[13,15–18] A synthetic quinazolinone conjugated indole acetamide was reported to have good cytotoxicity (IC_{50}s = 15.42, 75.35, and 137.3 μM) on HCT116, HT29, and HCA7 cancer cells (Fig. 1-III).[19] Moreover some synthetic indole-*N*-acetamides containing methyl (*E*)-2-cyanobut-2-enoate were reported to have IC_{50} values of 14–29.2 μM against A549 cells (Fig. 1-IV).[20]

Therefore, we designed novel benzothiazole-indole acetamides **9a–n** (Fig. 1) through a molecular fragmentation hybridization approach as anticancer agents. So far, many indole derivatives bearing divers amide substitutions on different positions of indole ring were evaluated,[19,21–23] and indole-*N*-acetamides have been the subject of less studies. In this study we aimed to investigate the anticancer activity of 2-(3-(benzo[*d*]thiazol-2-yl)-1*H*-indol-1-yl)-*N*-substituted acetamides **9a–n** (Fig. 1) and evaluate their antiproliferative activity against cancer cell lines. The effects of the most potent compound on cell cycle distribution and induction of apoptosis of cancer cells were also evaluated. Drug-likeness, pharmacokinetic, and toxicity properties were assessed *in silico*. Finally, molecular docking analysis was also performed.

2. Results and discussion

2.1. Synthesis

The step-by-step synthesis of the new 2-(3-(benzo[*d*]thiazol-2-yl)-1*H*-indol-1-yl)-*N*-substituted acetamides (**9a–n**) is outlined in Scheme 1. The synthesis commenced with the formation of the Vilsmeier reagent by combining phosphorus oxychloride with *N*,*N*-dimethylformamide (DMF, **1**) under controlled cooling. This reactive intermediate was subsequently treated with indole **2**, yielding 1*H*-indole-3-carbaldehyde **3** *via* Vilsmeier–Haack formylation. In the second step, the nucleophilic substitution reaction between chloroacetyl chloride **5** and the corresponding amine derivative **4a–n** in DMF at room temperature (r.t) led to the formation of 2-chloro-*N*-substituted acetamides **6a–n**. Next, 1*H*-indole-3-carbaldehyde **3** and acetamide derivatives **6a–n**

Table 1 The antiproliferative effect of the synthesized benzothiazoles-indole acetamides (**9a–n**)

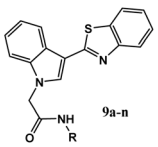

Comp.	R	IC_{50}[a] (μM) A549[b]	SW480[c]	HepG2[d]
9a		>200	>200	>200
9b		>200	>200	>200
9c		36.1 ± 2.6	37.2 ± 3.7	17.1 ± 1.9
9d	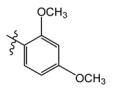	7.9 ± 1.6	16.1 ± 0.5	9.3 ± 2.2
9e		>200	>200	>200
9f		>200	>200	>200
9g		65.0 ± 2.8	44.8 ± 7.9	179.7 ± 4.5
9h		40.7 ± 6.0	49.8 ± 7.2	>200
9i		>200	>200	>200
9j		27.0 ± 2.3	29.0 ± 5.4	>200
9k		101.8 ± 4.5	180.3 ± 3.3	>200
9l		78.7 ± 3.2	74.0 ± 0.7	>200
9m		68.7 ± 4.0	53.5 ± 4.6	>200
9n		12.8 ± 0.3	16.8 ± 2.5	>200
Cisplatin	—	5.7 ± 1.6	15.2 ± 0.3	14.3 ± 1.9

[a] Mean ± SD of 3–4 independent replicates. [b] A549; adenocarcinomic human alveolar basal epithelial cells. [c] SW480; primary colon cancer cells. [d] HepG2; human hepatoma cells.

were reacted in the presence of anhydrous potassium carbonate. This step afforded 2-(3-formyl-1*H*-indol-1-yl)-*N*-substituted acetamide derivatives **7a–n** through a condensation process. Finally, compounds **7a–n** were condensed with 2-aminothiophenol **8** in the presence of sodium metabisulfite ($Na_2S_2O_5$) at 150 °C to acquire the target 2-(3-(benzo[*d*]thiazol-2-yl)-1*H*-indol-1-yl)-*N*-substituted acetamides **9a–n**, which were subsequently purified by recrystallization. The structures of final benzothiazole-indole-acetamides were confirmed by IR, ^{1}H NMR, ^{13}C NMR, and elemental analyses.

2.2. *In vitro* antiproliferative activity against cancer cells

The antiproliferative effects of the synthesized 2-(3-(benzo[*d*]thiazol-2-yl)-1*H*-indol-1-yl)-*N*-substituted acetamides were evaluated against A549 (human lung cancer), SW480 (human colon cancer), and HepG2 (human liver cancer) cell lines. The calculated IC_{50} values are presented in Table 1. Cisplatin was used as the positive control. Derivatives **9c**, **9d**, and **9g** demonstrated antiproliferative activity against the three A549, SW480, and HepG2 cancer cells, while **9h**, **9j**, **9k**, **9l**, **9m**, and **9n** exhibited activity against A549 and SW480 cells. Compounds **9a**, **9b**, **9e**, **9f**, and **9i** did not exhibit any activity over the cells at the tested concentrations. Compound **9d**, which contains a 2,4-dimethoxyphenyl group, was identified as the most potent derivative, with IC_{50} values of 7.9 ± 1.6 μM against A549 cells, and 16.1 ± 0.5 μM against SW480 cells, making it comparable to cisplatin. Moreover, **9d** showed an IC_{50} value of 9.3 ± 2.2 against HepG2, which was better than that of cisplatin with an IC_{50} values of 14.3 ± 1.9 μM. The second most effective compound was **9n**, which features a 4-ethylphenyl group, with IC_{50} values of 12.8 ± 0.3 μM for A549 cells and 16.8 ± 2.5 μM for SW480 cells. Moreover, compound **9j**, substituted with 3-nitrophenyl, also showed good antiproliferative activity on A549 and sw480 (IC_{50}s = 27.0 ± 2.3 and 29.0 ± 5.4 μM). Compound **9c** bearing a 3-chlorophenyl group had an IC_{50} value of 17.1 ± 1.9 μM on HepG2 cells. Derivatives **9c**, **9g**, **9h**, **9k**, **9l**, and **9m**, containing 3-chlorophenyl, phenethyl, *m*-tolyl, 2,4-dichlorophenyl, 4-bromophenyl, and *m*-tolyl substitutions, respectively, exhibited antiproliferative activity with IC_{50} values ranging from 36.1 to 180.3 μM against A549 and sw480 cells.

The antiproliferative activity of the synthesized compounds varies notably based on the nature and position of the substituent groups attached to the acetamide moiety. The data suggest that both electronic effects and steric factors of these substituents greatly influence their ability to inhibit cell proliferation. According to the results, a detailed structure–activity relationship has been established (Fig. 2).

Changing the phenyl substitution in the inactive **9e** to the phenethyl resulted in **9g** showing antiproliferative activity against both cancer cells. This indicates that increasing the distance between the acetamide moiety and the phenyl ring enhances compound's activity. The phenethyl group have more conformational flexibility than phenyl ring and may provide better accommodation in the binding site of the target receptor.

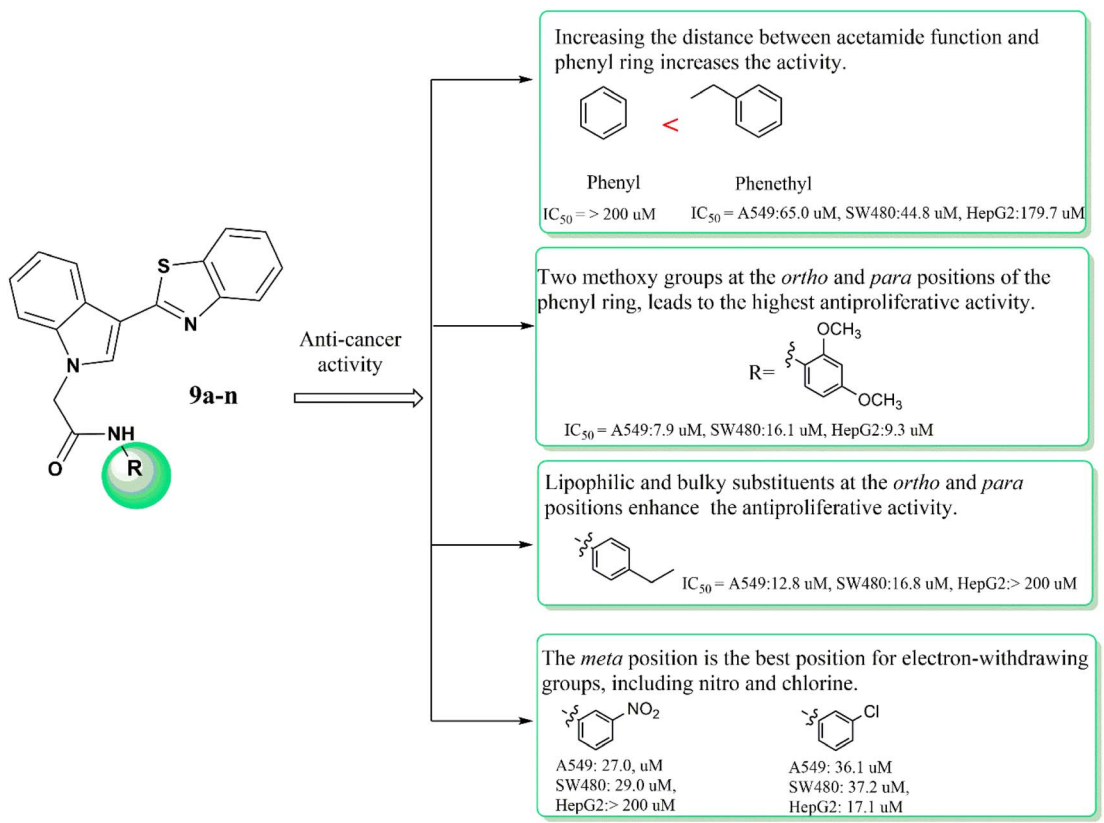

Fig. 2 Structure–activity relationship of the benzothiazoles-indole acetamides.

In the case of phenyl-substituted derivatives, it was observed that any substitution on the phenyl ring, excluding the 4-chloro, 2-fluoro, 4-methyl, and 2,4-dimethyl groups, resulted in the manifestation of an antiproliferative effect.

Methoxy groups, known for their electron-donating properties, may enhance the electron density of the aromatic ring, thereby potentially improving interactions such as hydrogen bonding, hydrophobic interactions, and π–π stacking with biological targets. Compound **9d**, which incorporates two methoxy groups at the *ortho* and *para* positions of the phenyl group, exhibited the highest antiproliferative activity.

The most advantageous position for the placement of electron-withdrawing groups, including nitro and chlorine, on the phenyl ring appears to be the *meta* position. This phenomenon is exemplified by compounds **9c** and **9j**, which contain chlorine and nitro moieties in the *meta* position, respectively, and exhibit moderate antiproliferative activity. Moreover, the incorporation of lipophilic and bulky substituents at the *ortho* and *para* positions of the phenyl group is posited to enhance antiproliferative activity against A549 and SW480. For instance, embedding a more lipophilic and bulky bromine atom at the *para* position, as illustrated in compound **9l**, resulted in a significant increase in activity compared to the inactive derivative **9a**, which features a chlorine substituent at the same position. Additionally, an increase in the number of chlorine atoms, as observed in compound **9k**, which contains chlorine atoms at the *ortho* and *para* positions, correlates with an enhancement in activity attributed to increased lipophilicity. This trend is further supported by the findings related to compound **9n**, wherein the introduction of a large and lipophilic ethyl group positions this compound as the second most active derivative in the studied series. The data suggest that even subtle alterations in the position and nature of substituents on the phenyl ring have a profound impact on biological activity, likely through modifications in molecular conformation and interactions with relevant biological targets.

2.3. *In vitro* cytotoxic activity against normal cells

The cytotoxic effects of derivative **9d** and **9n**, demonstrating the highest antiproliferative activity, were evaluated using MRC-5, a normal human cell line, to investigate the safety of the compounds. Cisplatin served as a positive control for comparative analysis. The calculated selectivity indexes (SI), as detailed in Table 2, revealed that **9d** exhibited markedly greater selectivity for the three cancer cells in comparison to the normal cell line. Compound **9n** did not show selectivity for HepG2 cells. Compound **9d** demonstrated higher selectivity, with SI values of 9.2, 4.5, and 7.8 for A549, SW480, and HepG2, respectively, while **9n** exposed SI values of 7.6, 5.8, and <0.4. Both derivatives showed considerably lower toxicity on the normal cells than cisplatin.

Table 2 The cytotoxicity of **9d**, **9n**, and cisplatin on the normal MRC-5 cells

		SI[c]		
Compound	IC_{50}[a] (μM) MRC-5[b]	A549	SW480	HepG2
9d	72.7 ± 3.2	9.2	4.5	7.8
9n	96.9 ± 6.9	7.6	5.8	<0.4
Cisplatin	18.3 ± 2.1	3.2	1.2	1.3

[a] Values are expressed as mean ± SD of three independent replicates. [b] MRC-5: human fetal lung fibroblast cells. [c] SI: selectivity index = IC_{50} of a compound in a normal cell line/IC_{50} of the same compound in a cancerous cell line.

2.4. Cell cycle arrest

To evaluate the impact of compound **9d** on cell cycle progression in A549 cells, a propidium iodide (PI) staining-assay was performed. After treating the cells for 48 h with 7.9 μM of **9d**, we observed a 1.9-fold increase in the number of cells in the G2/M phase compared to the untreated control cells ($p < 0.01$). This increase was accompanied by a significant decrease in the G0/G1 phase ($p < 0.001$). Additionally, the population of cells in the S phase showed a slight increase, which was not statistically significant compared to the control cells (Fig. 3). These findings

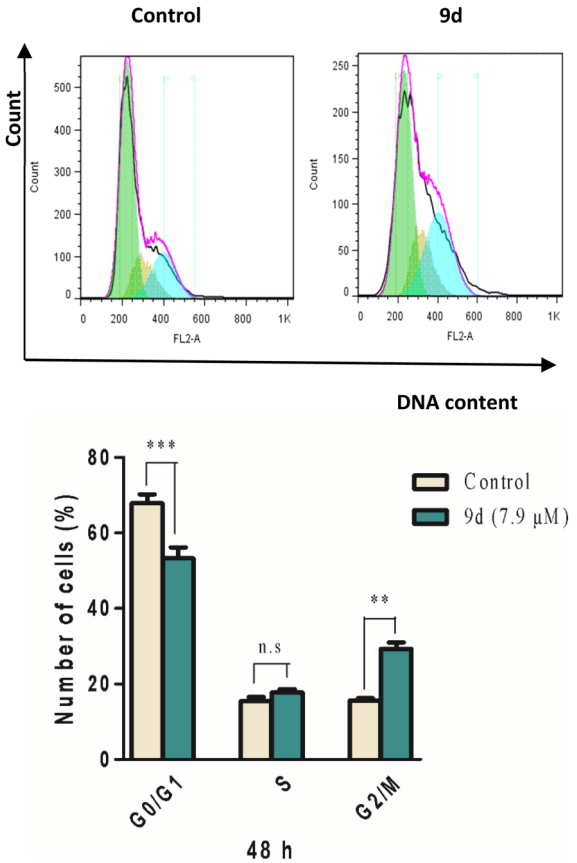

Fig. 3 Flow cytometry detection of cell cycle progression of A549 cells after treatment with compound **9d** for 48 h. The data are expressed as the mean ± standard deviation (SD) from three independent experiments. The significance levels are indicated as follows: n.s indicates non-significant; $^{**}p < 0.01$; and $^{***}p < 0.001$. These values were obtained using one-way ANOVA followed by Tukey's *post hoc* test to compare the percentages of treated cells with control cells.

indicate that compound **9d** significantly induces cell cycle arrest in the G2/M phase of A549 cells.

2.5. Apoptosis induction

The induction of apoptosis by compound **9d** in A549 cells was evaluated over a 48 hour period using flow cytometry. For this assessment, Annexin V conjugated with fluorescein isothiocyanate (FITC) and propidium iodide (PI) were used as markers to detect apoptotic events. Flow cytometry plots illustrating the staining patterns of Annexin V-FITC and PI show the pathways of cell death, as depicted in Fig. 4. The quadrants in the diagrams are interpreted as follows: Q1 (Annexin−/PI+) indicates necrotic cells, Q2 (Annexin+/PI+) indicates late

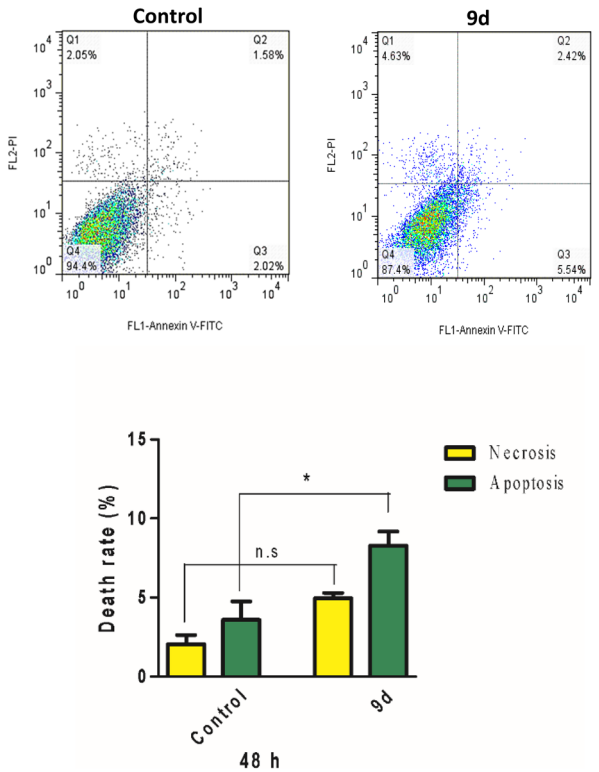

Fig. 4 Representation of the induced cell apoptosis by compound **9d**. Scatter plots were obtained by flow cytometery detection of Annexin V-FITC/PI staining on the A549 cells treated with 7.9 μM concentration of **9d** for 48 h. The data are expressed as the mean ± standard deviation (SD) from three independent experiments. The significance levels are indicated as follows: n.s indicates non-significant; and *$p < 0.05$. These values were obtained using one-way ANOVA followed by Tukey's *post hoc* test to compare the percentages of treated cells with control cells.

Table 3 The drug-likeness prediction results for **9d** and **9n**

	Drug-likeness				
Code	Lipinski	Ghose	Veber	Egan	Muegge
9d	Yes	Yes	Yes	Yes	No
9n	Yes	No	Yes	Yes	No

Table 4 *In silico* absorption and distribution profiling of **9d** and **9n**

	Absorption				Distribution	
Code	Human Intestinal Absorption HIA (percentage)	*In vitro* Caco-2[a] cell permeability (nm s^{-1})	*In vitro* MDCK[b] cell permeability (nm s^{-1})	P-gp[c] inhibition	*In vitro* plasma protein binding (percentage)	*In vivo* blood–brain barrier penetration (C.brain/C.blood)
	0–20 (poor)	<4 (low)	<25 (low)		>90 (strongly)	<0.1 (low)
	20–70 (moderate)	4–70 (moderate)	25–500 (moderate)		<90 (weakly)	0.1–2 (moderate)
	70–100 (well)	>70 (high)	>500 (high)			>2 (high)
9d	97.13	28.78	1.15	Inhibitor	92.07	0.97
9n	97.46	29.47	48.37	Inhibitor	94.69	0.37

[a] Caco-2: human colorectal carcinoma cells. [b] MDCK: Maden-Darby canine kidney. [c] P-gp: P-glycoprotein.

apoptotic cells, Q3 (Annexin+/PI−) indicates early apoptotic cells, and Q4 (Annexin−/PI−) indicates viable, non-apoptotic cells. In the control cells, late and early apoptotic cells comprised 1.58% and 2.02%, respectively. However, treatment with compound **9d** at a concentration of 7.9 μM resulted in an increase in late and early apoptotic cells to 2.42% and 5.54%, respectively. Compound **9d** caused a significant increase (2.3-fold) in the total apoptotic cell rates (Q2 + Q3) ($p < 0.05$). Additionally, the number of necrotic cells (Q1) experienced a slight increase in the presence of compound **9d**, though this change was not statistically significant compared to the control cells. These findings demonstrate that compound **9d** effectively induces apoptosis in A549 cells.

2.6. *In silico* prediction of drug-likeness, pharmacokinetic and toxicity properties

The drug-likeness (including Lipinski,[24] Ghose, Veber, Egan, and Muegge rules) and pharmacokinetics profiles (human intestinal absorption, *in vitro* Caco-2 cell permeability, *in vitro* MDCK cell permeability, P-gp inhibition, *in vitro* plasma protein binding, and *in vivo* BBB penetration, the cytochrome P450 enzymes inhibition/substrate and water solubility) were predicted for **9d** and **9n** derivatives that showed the highest anti-proliferative activities against cancer cells. The results are presented in Tables 3–5.

As it is reported in Table 3, **9d** satisfied all the criteria except for the Muegge rule, while **9n** failed to comply with the Ghose and Muegge rules. Therefore, **9d** had more qualified drug-likeness scores than **9n**.

The data in Table 4 suggested that both **9d** and **9n** had high intestinal absorption. They are predicted to have moderate permeability across the blood–brain barrier, suggesting that they may cause minimal neurotoxicity. Additionally, both compounds showed high plasma protein binding. They exhibited medium permeability in Caco-2 and low permeability in MDCK cells. It is suggested that **9d** and **9n** might reverse multidrug resistance (MDR) as they are predicted to exert an inhibitory effect on the P-gp pump. MDR is the main cause of chemotherapy ineffectiveness in cancer treatment, primarily due to the overexpression of drug efflux pumps, particularly P-gp, in cancer cells.[25–27] Therefore, administration of **9d** and **9n** with the common anticancer drugs may not only lead to a synergistic anticancer effect but also help reverse the MDR associated with the P-gp pump.

The compounds were predicted not to inhibit CYP2D6, CYP3A4, CYP2C19, and CYP2C9, indicating no risk for interaction with drugs metabolized by the liver enzymes. Compounds **9d** and **9n** had low water solubility; therefore, they are less likely to be excreted by the urinary system. Unlike **9n**, compound **9d** is a good substrate for the CYP3A4 enzyme; therefore, **9d** may be better excreted as a result of being metabolized by the cytochrome P450 enzyme as compared with **9n** (Table 5).

The predicted toxicity properties contain mutagenicity against histidine synthesis (Ames test), carcinogenicity with the mouse (Carcino-Mouse) and rat (Carcino-Rat), human ether-a-go-go inhibition (hERG-inhibition), *in vitro* Ames test with (+S9) and without (−S9) metabolic activation in TA100 and TA1535 strains rat liver (TA100-10RLI, TA100-NA, TA1535-10RLI, and TA1535-NA). The results are listed in Table 6. Compound **9d** showed negative Ames mutagenicity to all the strains, while **9n** was predicted to be mutagenic against the TA100-10RLI strain. Moreover, **9d** showed negative carcinogenicity for the rat and mouse, but **9n** presented positive carcinogenicity for the mouse. The compounds had a medium risk for hERG inhibition. Overall, compound **9d** was predicted to have no carcinogenic and mutagenic effects, while **9n** showed some degree of mutagenicity and carcinogenicity. Causing carcinogenic and mutagenic effects is a limitation for **9n**, therefore, **9d** is more likely to be considered as a lead compound compared to **9n**.

Taking into account all the above-mentioned results, **9d** was predicted to have better drug-likeness, pharmacokinetic, and toxicity properties as compared to **9n**.

2.7. Molecular docking analysis

The epidermal growth factor receptor (EGFR) tyrosine kinase plays a key role in signal transduction pathways and regulation of the cell cycle and motility of the cell.[28] Mutations or over-expression of EGFR stimulates cell proliferation, angiogenesis, anti-apoptosis and metastasis causing a variety of epidermal carcinomas. Consequently, inhibition of EGFR is an attractive approach for the development of new anticancer agents.[29] Many synthetic derivatives of benzothiazole[30,31] and indole[17] has been reported as EGFR inhibitors.

Table 5 *In silico* metabolism and excretion profiling of **9d** and **9n**

	Metabolism						Excretion
							Pure water solubility ($mg\ L^{-1}$)
Code	CYP2C19 inhibition	CYP2C9 inhibition	CYP2D6 inhibition	CYP2D6 substrate	CYP3A4 inhibition	CYP3A4 substrate	Low: <10; moderate: 10–1000; high: >1000
9d	Non	Non	Non	Non	Non	Substrate	0.09
9n	Non	Non	Non	Non	Non	Weakly	0.02

Table 6 *In silico* toxicity prediction results for **9d** and **9n**

Code	Ames_test	Carcino_Mouse	Carcino_Rat	hERG_inhibition	TA100_10RLI	TA100_ NA	TA1535_10RLI	TA1535_NA
9d	Non-mutagen	Negative	Negative	Medium-risk	Negative	Negative	Negative	Negative
9n	Mutagen	Positive	Negative	Medium-risk	Positive	Negative	Negative	Negative

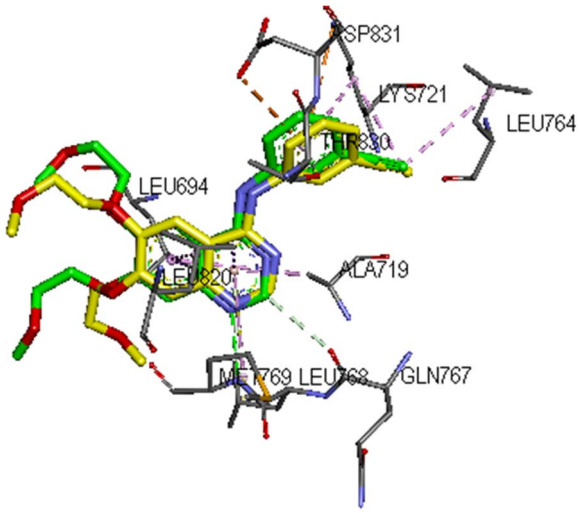

Fig. 5 Superimposed docked conformation (yellow) of erlotinib with the X-ray crystal conformation (green) in the binding site of EGFR (PDB ID: 1M17). Hydrogen bonding, electrostatic, and hydrophobic interactions are displayed as green, orange, and pink dashes, respectively.

To predict the binding mode and affinity of the most active derivative **9d** in the EGFR binding site (PDB ID: 1M17), molecular docking analysis were performed. The innate ligand erlotinib was first docked into the binding site of EGFR (ΔG = −7.44 kcal mol^{-1}). The docked conformation of erlotinib was superimposed on the X-ray crystal conformation (Fig. 5). An RMSD value of 0.91 Å proved the docking protocol reproducibility. Compound **9d** displayed a binding energy value of −8.86 kcal mol^{-1}, which is more negative than that of erlotinib. This suggests that **9d** is predicted to interact more strongly and is positioned more tightly within the binding site of EGFR compared to erlotinib.

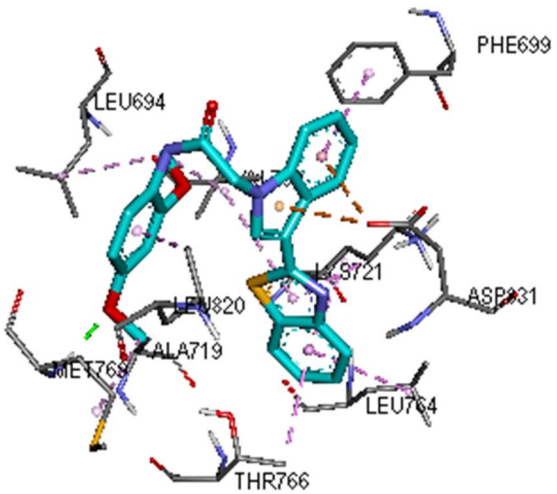

Fig. 6 Interactions of **9d** (cyan) in the binding site of EGFR (PDB ID: 1M17). Hydrogen bonding, electrostatic, and hydrophobic interactions are displayed as green, orange, and pink dashes, respectively.

Compound **9d** (Fig. 6) was able to establish a strong hydrogen bonding interaction with MET769 in the hinge region through the 4-methoxy substitution. The benzothiazole nucleus provided hydrophobic interactions with LYS721, LEU764, and THR766, while the indole group formed electrostatic and hydrophobic interactions with ASP831 and PHE699, respectively. Moreover, the 2,4-dimethoxyphenyl ring occupied the hydrophobic pocket comprising LEU694, val702, ALA719, MET769, and LEU820 residues.

3. Conclusions

Fourteen new benzothiazole-indole acetamide hybrids were designed and synthesized as anticancer agents. The synthesized derivatives were evaluated *in vitro* for their antiproliferative activities against A549, SW480, and HepG2 cancer cells. Compound **9d** was the most potent derivative, exhibiting high antiproliferative activities against A549, SW480, and HepG2 cell lines with IC_{50} values of 7.9, 16.1, and 9.3 μM, respectively. In A549 and SW480 cells, the antiproliferative activity of **9d** was comparable to cisplatin with IC_{50} values of 5.7 and 15.2 μM, while, in the case of HepG2 cells it was even superior to cisplatin with an IC_{50} value of 14.3 μM. In addition, compound **9n** ($IC_{50=}$ 12.8 and 16.8 μM) also demonstrated good antiproliferative activity against A549, SW480 cells, however, it did not show activity against HepG2 cells. Compounds **9d** showed more cytotoxic selectivity toward cancerous cells over the normal cell line MRC-5 as compared to cisplatin. Cell cycle analysis revealed that **9d** can arrest A549 cell growth at G2/M phase by 1.9-fold greater than the untreated control cells. Moreover, compound **9d** induced apoptosis in A549 cells by 2.3 times more than the control cells. *In silico* studies revealed that compound **9d** is predicted to have more acceptable drug-likeness, pharmacokinetic, and toxicity profiling than **9n**. Compound **9d** was docked into the EGFR binding site and displayed tough interactions. Finally, this work presents compound **9d** as a candidate that can be further developed as a promising anticancer drug.

4. Materials and methods

4.1. Apparatus

All chemicals and reagents were of commercial grade. The reactions were monitored using pre-coated aluminum sheet thin layer chromatography (TLC) plates (MERCK, silica gel 60-F254). The IR spectra were obtained on a Nicolet FT-IR Magna

550 spectrometer (KBr disks). The nuclear magnetic resonance (NMR) spectra were attained by a Bruker DRX-500 NMR spectrometer (^{1}H: 600 MHz, ^{13}C: 151 MHz) using DMSO-d_6 as the solvent. Chemical shifts (δ) and J values are expressed in parts per million (ppm) and hertz (Hz), respectively. Melting points were measured with a Barnstead IA9300 system (Electrothermal, UK), and are uncorrected. Elemental analyses were done by a PerkinElmer 2400 CHN Elemental Analyzer and were within ± 0.4% of the theoretical values for C, H, and N.

4.2. Synthesis

4.2.1. Preparation of indole-3-carbaldehyde (3). Phosphorus oxychloride ($POCl_3$, 100 mmol, 9.5 mL) was added dropwise to a stirred amount of cooled (0–5 °C) *N*,*N*-dimethylformamide **1** (DMF, 30 mL). The solution was stirred in the ice bath for 30 min. Then, 1*H*-indol **2** (50 mmol, 6 g) dissolved in DMF was added to the solution and stirred at r.t for 1 h. Upon completion of the reaction, the mixture was cooled, and a solution of ice water and sodium hydroxide (30%) was added gradually until the pH reached 8.0. The final product **3** was then isolated by filtration (1). Yield: 83%.

4.2.2. Preparation of 2-chloro-*N*-substituted acetamides (6a–n). A solution of aniline derivatives (**4a–n**) (2 mmol) in DMF (10 mL) was stirred in an ice bath for 30 min. Subsequently, chloroacetyl chloride **5** (2 mmol, 0.16 mL) was added dropwise to the cold solution while stirring. The reaction mixture was then allowed to stir at r.t, and monitored TLC (petroleum ether/ethyl acetate, the ratio was varied from 4 : 1 to 2 : 1). Once the reaction was complete, the mixture was poured into ice-cold water, and the resulting precipitate was collected by filtration to yield the final products (**6a–n**) (2). Yield: 87–96%.

4.2.3. Preparation of 2-(3-formyl-1*H*-indol-1-yl)-*N*-substituted acetamides (7a–n). A solution of indole-3-carbaldehyde **3** (1.5 mmol, 0.2 g), anhydrous potassium carbonate (K_2CO_3, 1.8 mmol, 0.25 g) and corresponding acetamide derivatives **6a–n** (1.5 mmol) in dry DMF (3 mL) was stirred for 16 h at r.t. After completion of the reaction (checked by TLC; petroleum ether/ethyl acetate, the solvent ratio was varied from 4 : 1 to 3 : 1), the mixture was poured into water, then the precipitated **7a–n** was filtered. Yield: 79–90%.

4.2.4. Preparation of 2-(3-(benzo[*d*]thiazol-2-yl)-1*H*-indol-1-yl)-*N*-substituted acetamides (9a–n). A solution of corresponding indole derivatives **7a–n** (1 mmol) and 2-aminothiophenol **8** (1.2 mmol, 0.15 g) in DMF (3 mL) and sodium metabisulfite ($Na_2S_2O_5$, 1.2 mmol, 0.23 g) was refluxed at 150 °C for 3 h. The progress of the reaction was monitored by TLC (petroleum ether/ethyl acetate; 2 : 1). After completion of the reaction, it was cooled and poured in chilled water. The acquired precipitate was recrystallized in ethyl acetate to yield the corresponding pure final product **9a–n**. Yield: 61–95%.

*4.2.4.1. 2-(3-(Benzo[d]thiazol-2-yl)-1H-indol-1-yl)-N-(4-chlorophenyl)acetamide **9a**.* Pale yellow solid; yield: 87%; mp: 151–153 °C; IR (KBr, ν_{max}): 3334 (NH), 3035 (C–H aromatic), 2940 (CH aliphatic), 1669 (C=O) cm^{-1}; ^{1}H NMR (600 MHz, DMSO-d_6) δ 10.70 (s, 1H, CONH), 8.41 (dd, J = 6.0, 3.2 Hz, 1H, Ar–H), 8.36 (s, 1H, H-2 indole), 8.07 (d, J = 7.9 Hz, 1H, Ar–H), 7.98 (d, J = 8.1 Hz, 1H, Ar–H), 7.65 (d, J = 8.6 Hz, 2H, Ph-H), 7.58 (dd, J = 6.1, 3.2 Hz, 1H, Ar–H), 7.50 (t, J = 7.7 Hz, 1H, Ar–H), 7.40–7.35 (m, 3H, Ar–H), 7.31 (dd, J = 6.1, 3.1 Hz, 2H, Ar–H), 5.24 (s, 2H, NCH_2CO) ppm; ^{13}C NMR (151 MHz, DMSO-d_6) δ 166.1 (C=O), 162.5 (C-3a benzo[*d*]thiazole), 153.9 (C-2 benzo[*d*]thiazole), 137.8, 137.6, 133.3, 133.1, 129.0, 127.4, 126.4, 125.1, 124.6, 123.2, 122.0, 121.9, 121.8, 121.1, 121.0, 111.0, 110.2, 49.5 (CH_2, NCH_2CO) ppm; anal. calcd for $C_{23}H_{16}ClN_3OS$: C, 66.10; H, 3.86; N, 10.05; found: C, 66.27; H, 4.01; N, 10.19.

*4.2.4.2. 2-(3-(Benzo[d]thiazol-2-yl)-1H-indol-1-yl)-N-(2-fluorophenyl)acetamide **9b**.* White solid; yield: 65%; mp: 135–137 °C; IR (KBr, ν_{max}): 3341 (NH), 3050 (C–H aromatic), 2955 (CH aliphatic), 1674 (C=O) cm^{-1}; ^{1}H NMR (600 MHz, DMSO-d_6) δ 10.32 (s, 1H, CONH), 8.45–8.42 (m, 1H, Ar–H), 8.37 (s, 1H, H-2 indole), 8.07 (d, J = 7.9 Hz, 1H, Ar–H), 7.99 (d, J = 8.1 Hz, 1H, Ar–H), 7.93 (td, J = 7.9, 3.4 Hz, 1H, Ar–H), 7.60–7.56 (m, 1H, Ar–H), 7.50 (t, J = 7.7 Hz, 1H, Ar–H), 7.38 (t, J = 7.6 Hz, 1H, Ar–H), 7.35–7.29 (m, 3H, Ar–H), 7.19–7.13 (m, 2H, Ar–H), 5.32 (s, 2H, NCH_2CO) ppm; ^{13}C NMR (151 MHz, DMSO-d_6) δ 166.3 C=O, 162.3 (C-3a benzo[*d*]thiazole), 154.3, 153.7 (C-2 benzo[*d*]thiazole), 152.7, 137.3, 133.2, 133.0, 126.2, 125.0, 124.5, 124.4, 123.7, 123.1, 121.8, 121.7, 121.6, 121.0, 115.7, 115.5, 110.8, 110.0, 49.2 (CH_2, NCH_2CO) ppm; anal. calcd for $C_{23}H_{16}FN_3OS$: C, 68.81; H, 4.02; N, 10.47; found: C, 68.96; H, 4.17; N, 10.61.

*4.2.4.3. 2-(3-(Benzo[d]thiazol-2-yl)-1H-indol-1-yl)-N-(3-chlorophenyl)acetamide **9c**.* White solid; yield: 83%; mp: 165–167 °C; IR (KBr, ν_{max}): 3331 (NH), 3035 (C–H aromatic), 2955 (CH aliphatic), 1669 (C=O) cm^{-1}; ^{1}H NMR (600 MHz, DMSO-d_6) δ 10.05 (s, 1H, CONH), 8.44–8.41 (m, 1H), 8.38 (s, 1H, H-2 indole), 8.07 (d, J = 7.8 Hz, 1H), 7.99 (d, J = 8.0 Hz, 1H), 7.76 (dd, J = 8.2, 1.6 Hz, 1H), 7.62–7.57 (m, 1H), 7.55–7.47 (m, 2H), 7.40–7.30 (m, 4H), 7.21 (td, J = 7.7, 1.6 Hz, 1H), 5.33 (s, 2H, NCH_2CO) ppm; ^{13}C NMR (151 MHz, DMSO-d_6) δ 166.3 C=O, 162.3 (C-3a benzo[*d*]thiazole), 153.7 (C-2 benzo[*d*]thiazole), 137.3, 134.4, 133.1, 133.0, 129.6, 127.6, 126.6, 126.3, 126.2, 125.9, 125.0, 124.4, 123.1, 121.9, 121.7, 121.6, 121.0, 110.8, 110.0, 49.2 (CH_2, NCH_2CO) ppm; anal. calcd for $C_{23}H_{16}ClN_3OS$: C, 66.10; H, 3.86; N, 10.05; found: C, 66.28; H, 4.02; N, 10.22.

*4.2.4.4. 2-(3-(Benzo[d]thiazol-2-yl)-1H-indol-1-yl)-N-(2,4-dimethoxyphenyl)acetamide **9d**.* Purple solid; yield: 83%; mp: 151–153 °C; IR (KBr, ν_{max}): 3214 (NH), 3025 (CH aromatic), 2940 (CH aliphatic), 1663 (C=O) cm^{-1}; mp: 151–153 °C; ^{1}H NMR (600 MHz, DMSO-d_6) δ 9.57 (s, 1H, CONH), 8.44–8.41 (m, 1H), 8.35 (s, 1H, H-2 indole), 8.07 (d, J = 7.8 Hz, 1H), 7.99 (d, J = 8.0 Hz, 1H), 7.72 (d, J = 8.8 Hz, 1H), 7.60–7.57 (m, 1H), 7.50 (t, J = 7.6 Hz, 1H), 7.38 (t, J = 7.6 Hz, 1H), 7.35–7.30 (m, 2H), 6.64 (d, J = 2.7 Hz, 1H), 6.47 (dd, J = 8.9, 2.7 Hz, 1H), 5.26 (s, 2H, NCH_2CO), 3.85 (s, 3H, OCH_3, C-2), 3.73 (s, 3H, OCH_3, C-4) ppm; ^{13}C NMR (151 MHz, DMSO-d_6) δ 165.5 C=O, 162.4 (C-3a benzo[*d*]thiazole), 157.0 (Cq, Ar-OCH_3), 153.7 (C-2 benzo[*d*]thiazole), 151.3, 137.3, 133.1, 133.0, 126.2, 125.0, 124.4, 123.3, 123.0, 121.8, 121.7, 121.6, 121.0, 119.8, 110.8, 109.9, 104.1, 98.9, 55.8 (OCH_3), 55.3 (OCH_3), 49.3 (CH_2, NCH_2CO) ppm; anal. calcd for $C_{25}H_{21}N_3O_3S$: C, 67.70; H, 4.77; N, 9.47; found: C, 67.84; H, 4.93; N, 9.65.

*4.2.4.5. 2-(3-(Benzo[d]thiazol-2-yl)-1H-indol-1-yl)-N-phenylacetamide **9e**.* White solid; yield: 95%; mp: 145–147 °C; IR (KBr,

ν_{max}): 3321 (NH), 3035 (C–H aromatic), 2950 (CH aliphatic), 1661 (C=O) cm^{-1}; ^1H NMR (600 MHz, DMSO-d_6) δ 10.48 (s, 1H, CONH), 8.44–8.41 (m, 1H), 8.37 (s, 1H, H-2 indole), 8.07 (d, J = 7.6 Hz, 1H), 7.99 (d, J = 8.0 Hz, 1H), 7.61 (dd, J = 8.5, 1.3 Hz, 2H), 7.59–7.55 (m, 1H), 7.50 (ddd, J = 8.2, 7.2, 1.2 Hz, 1H), 7.38 (ddd, J = 8.2, 7.2, 1.2 Hz, 1H), 7.35–7.29 (m, 4H), 7.08 (tt, J = 7.4, 1.2 Hz, 1H), 5.23 (s, 2H, NCH_2CO) ppm; ^{13}C NMR (151 MHz, DMSO) 165.7 C=O, 162.4 (C-3a benzo[*d*]thiazole), 153.7 (C-2 benzo[*d*]thiazole), 138.7, 137.4, 133.2, 133.0, 128.9, 126.2, 124.9, 124.4, 123.6, 123.0, 121.8, 121.7, 121.6, 121.0, 119.2, 110.8, 109.9, 49.4 (CH_2, NCH_2CO) ppm; anal. calcd for $C_{23}H_{17}N_3OS$: C, 72.04; H, 4.47; N, 10.96; found: C, 72.19; H, 4.63; N, 11.12.

4.2.4.6. 2-(3-(Benzo[d]thiazol-2-yl)-1H-indol-1-yl)-N-(p-tolyl) acetamide ***9f***. White solid; yield: 74%; mp: 132–134 °C; IR (KBr, ν_{max}): 3294 (NH), 3005 (CH aromatic), 2925 (CH aliphatic), 1671 (C=O) cm^{-1}; ^1H NMR (600 MHz, DMSO-d_6) δ 10.41 (s, 1H, CONH), 8.43–8.39 (m, 1H), 8.35 (s, 1H, H-2 indole), 8.06 (d, J = 8.0 Hz, 1H), 7.98 (d, J = 8.1 Hz, 1H), 7.56 (dd, J = 6.6, 2.8 Hz, 1H), 7.49 (dd, J = 8.0, 6.4 Hz, 3H), 7.38 (t, J = 7.6 Hz, 1H), 7.33–7.29 (m, 2H), 7.13 (d, J = 8.2 Hz, 2H), 5.20 (s, 2H, NCH_2CO), 2.25 (s, 3H, CH_3) ppm; ^{13}C NMR (151 MHz, DMSO-d_6) δ 165.5 C=O, 162.4 (C-3a benzo[*d*]thiazole), 153.6 (C-2 benzo[*d*]thiazole), 137.4, 136.2, 133.2, 133.0, 132.7, 129.3, 126.3, 125.0, 124.4, 123.0, 121.9, 121.7, 121.6, 121.0, 119.7, 110.8, 110.0, 49.4 (CH_2, NCH_2CO), 20.5 (CH_3) ppm; anal. calcd for $C_{24}H_{19}N_3OS$: C, 72.52; H, 4.82; N, 10.57; found: C, 72.68; H, 4.98; N, 10.72.

4.2.4.7. 2-(3-(Benzo[d]thiazol-2-yl)-1H-indol-1-yl)-N-phen-ethylacetamide ***9g***. Cream solid; yield: 61%; mp: 157–159 °C; IR (KBr, ν_{max}): 3224 (NH), 3015 (CH aromatic), 2980 (CH aliphatic), 1661 (C=O) cm^{-1}; ^1H NMR (600 MHz, DMSO-d_6) δ 8.43–8.36 (m, 2H, Ar–H and CONH), 8.26 (s, 1H, H-2 indole), 8.07 (d, J = 7.9 Hz, 1H), 7.98 (d, J = 8.1 Hz, 1H), 7.49 (ddd, J = 8.2, 7.2, 1.3 Hz, 1H), 7.41–7.36 (m, 2H), 7.31–7.27 (m, 4H), 7.23–7.19 (m, 3H), 4.95 (s, 2H, NCH_2CO), 3.35 (t, J = 7.3 Hz, 2H, NH–CH_2), 2.75 (t, J = 7.2 Hz, 2H, CH_2-Ph) ppm; ^{13}C NMR (151 MHz, DMSO-d_6) δ 166.7 C=O, 162.4 (C-3a benzo[*d*]thiazole), 153.7 (C-2 benzo[*d*]thiazole), 139.3, 137.1, 133.1, 133.0, 128.7, 128.4, 126.3, 126.2, 125.0, 124.4, 123.0, 121.9, 121.7, 121.6, 121.0, 110.8, 109.9, 49.0 (CH_2, NCH_2CO), 40.4 (CH_2, NH–CH_2), 35.0 (CH_2, CH_2-Ph) ppm; anal. calcd for $C_{25}H_{21}N_3OS$: C, 72.97; H, 5.14; N, 10.21; found: C, 73.13; H, 5.32; N, 10.38.

4.2.4.8. 2-(3-(Benzo[d]thiazol-2-yl)-1H-indol-1-yl)-N-(m-tolyl) acetamide ***9h***. Ream solid; yield: 74%; mp: 137–139 °C; IR (KBr, ν_{max}): 3310 (NH), 3020 (CH aromatic), 2930 (CH aliphatic), 1671 (C=O) cm^{-1}; ^1H NMR (600 MHz, DMSO-d_6) δ 10.41 (s, 1H, CONH), 8.42 (dd, J = 6.2, 3.0 Hz, 1H), 8.35 (s, 1H, H-2 indole), 8.07 (d, J = 7.9 Hz, 1H), 7.98 (d, J = 8.1 Hz, 1H), 7.56 (dd, J = 6.4, 2.9 Hz, 1H), 7.50 (t, J = 7.7 Hz, 1H), 7.45 (s, 1H), 7.38 (t, J = 7.7 Hz, 2H), 7.33–7.30 (m, 2H), 7.20 (t, J = 7.9 Hz, 1H), 6.90 (d, J = 7.6 Hz, 1H), 5.21 (s, 2H, NCH_2CO), 2.27 (s, 3H, CH_3) ppm; ^{13}C NMR (151 MHz, DMSO-d_6) δ 165.6 C=O, 162.4 (C-3a benzo[*d*]thiazole), 153.6 (C-2 benzo[*d*]thiazole), 138.6, 138.1, 137.4, 133.2, 133.0, 128.8, 126.3, 125.0, 124.4, 124.4, 123.1, 121.9, 121.7, 121.6, 121.0, 119.8, 116.4, 110.8, 110.0, 49.4 (CH_2, NCH_2CO), 21.2 (CH_3) ppm; anal. calcd for $C_{24}H_{19}N_3OS$: C, 72.52; H, 4.82; N, 10.57; found: C, 72.66; H, 5.01; N, 10.76.

4.2.4.9. 2-(3-(Benzo[d]thiazol-2-yl)-1H-indol-1-yl)-N-(2,4-di-methylphenyl)acetamide ***9i***. White solid; yield: 83%; mp: 166–168 °C; IR (KBr, ν_{max}): 3226 (NH), 3030 (CH aromatic), 2950 (CH aliphatic), 1669 (C=O) cm^{-1}; ^1H NMR (600 MHz, DMSO-d_6) δ 9.73 (s, 1H, CONH), 8.42 (dd, J = 6.7, 1.7 Hz, 1H), 8.36 (s, 1H, H-2 indole), 8.07 (d, J = 7.8 Hz, 1H), 7.98 (d, J = 7.7 Hz, 1H), 7.61–7.57 (m, 1H), 7.49 (ddd, J = 8.2, 7.2, 1.3 Hz, 1H), 7.38 (ddd, J = 8.2, 7.2, 1.1 Hz, 1H), 7.35–7.27 (m, 3H), 7.03 (s, 1H), 6.96 (d, J = 8.0 Hz, 1H), 5.24 (s, 2H, NCH_2CO), 2.23 (s, 3H, CH_3), 2.20 (s, 3H, CH_3) ppm; ^{13}C NMR (151 MHz, DMSO-d_6) δ 165.7 C=O, 162.4 (C-3a benzo[*d*]thiazole), 153.7 (C-2 benzo[*d*]thiazole), 137.3, 134.6, 133.2, 133.1, 133.0, 131.7, 130.9, 126.6, 126.3, 125.0, 124.9, 124.4, 123.0, 121.9, 121.7, 121.6, 121.0, 110.8, 109.9, 49.2 (CH_2, NCH_2CO), 20.5 (CH_3), 17.8 (CH_3) ppm; anal. calcd for $C_{25}H_{21}N_3OS$: C, 72.97; H, 5.14; N, 10.21; found: C, 73.16; H, 5.31; N, 10.38.

4.2.4.10. 2-(3-(Benzo[d]thiazol-2-yl)-1H-indol-1-yl)-N-(3-nitro-phenyl)acetamide ***9j***. Brown solid; yield: 77%; mp: 185–187 °C; IR (KBr, ν_{max}): 3351 (NH), 3050 (CH aromatic), 2970 (CH aliphatic), 1671 (C=O), 1561–1357 (NO_2) cm^{-1}; ^1H NMR (600 MHz, DMSO-d_6) δ 11.02 (s, 1H, CONH), 8.63 (d, J = 2.3 Hz, 1H), 8.43 (dd, J = 6.1, 3.2 Hz, 1H), 8.38 (s, 1H, H-2 indole), 8.07 (d, J = 7.9 Hz, 1H), 7.99 (d, J = 8.1 Hz, 1H), 7.95 (ddd, J = 7.5, 4.1, 2.1 Hz, 2H), 7.64 (t, J = 8.2 Hz, 1H), 7.60 (dd, J = 6.2, 3.2 Hz, 1H), 7.50 (t, J = 7.6 Hz, 1H), 7.38 (t, J = 7.5 Hz, 1H), 7.32 (dd, J = 6.1, 3.1 Hz, 2H), 5.31 (s, 2H, NCH_2CO) ppm; ^{13}C NMR (151 MHz, DMSO-d_6) δ 166.7 C=O, 162.4 (C-3a benzo[*d*]thiazole), 153.7 (C-2 benzo[*d*]thiazole), 148.0, 139.8, 137.5, 133.2, 133.0, 130.4, 126.3, 125.2, 124.9, 124.4, 123.1, 121.9, 121.7, 121.6, 121.0, 118.2, 113.4, 110.9, 110.1, 49.3 (CH_2, NCH_2CO) ppm; anal. calcd for $C_{23}H_{16}N_4O_3S$: C, 64.47; H, 3.76; N, 13.08; found: C, 64.62; H, 3.93; N, 13.24.

4.2.4.11. 2-(3-(Benzo[d]thiazol-2-yl)-1H-indol-1-yl)-N-(2,4-di-chlorophenyl)acetamide ***9k***. White solid; yield: 69%; mp: 189–191 °C; IR (KBr, ν_{max}): 3348 (NH), 3055 (CH aromatic), 2945 (CH aliphatic), 1669 (C=O) cm^{-1}; ^1H NMR (600 MHz, DMSO-d_6) δ 10.13 (s, 1H, CONH), 8.45–8.41 (m, 1H), 8.37 (s, 1H, H-2 indole), 8.07 (d, J = 7.9 Hz, 1H), 7.99 (d, J = 8.1 Hz, 1H), 7.80 (d, J = 8.8 Hz, 1H), 7.70 (d, J = 2.5 Hz, 1H), 7.61–7.56 (m, 1H), 7.50 (t, J = 7.6 Hz, 1H), 7.42 (dd, J = 8.8, 2.4 Hz, 1H), 7.38 (t, J = 7.6 Hz, 1H), 7.35–7.30 (m, 2H), 5.33 (s, 2H, NCH_2CO) ppm; ^{13}C NMR (151 MHz, DMSO-d_6) δ 166.5 C=O, 162.3 (C-3a benzo[*d*]thiazole), 153.7 (C-2 benzo[*d*]thiazole), 137.3, 133.6, 133.1, 133.0, 129.7, 129.1, 127.7, 127.2, 126.8, 126.2, 125.0, 124.4, 123.1, 121.9, 121.7, 121.6, 121.0, 110.8, 110.1, 49.2 (CH_2, NCH_2CO) ppm; anal. calcd for $C_{23}H_{15}Cl_2N_3OS$: C, 61.07; H, 3.34; N, 9.29; found: C, 61.24; H, 3.51; N, 9.42.

4.2.4.12. 2-(3-(Benzo[d]thiazol-2-yl)-1H-indol-1-yl)-N-(4-bromophenyl)acetamide ***9l***. Yellow solid; yield: 79%; mp: 197–199 °C; IR (KBr, ν_{max}): 3337 (NH), 3030 (C–H aromatic), 2960 (CH aliphatic), 1674 (C=O) cm^{-1}; ^1H NMR (600 MHz, DMSO-d_6) δ 10.63 (s, 1H, CONH), 8.41 (dd, J = 6.1, 3.2 Hz, 1H), 8.35 (s, 1H, H-2 indole), 8.06 (d, J = 7.8 Hz, 1H), 7.98 (d, J = 8.1 Hz, 1H), 7.60–7.54 (m, 3H), 7.53–7.47 (m, 3H), 7.38 (t, J = 7.6 Hz, 1H), 7.31 (dd, J = 6.1, 3.1 Hz, 2H), 5.23 (s, 2H, NCH_2CO) ppm; ^{13}C NMR (151 MHz, DMSO-d_6) δ 166.0 C=O, 162.4 (C-3a benzo[*d*]

thiazole), 153.7 (C-2 benzo[*d*]thiazole), 138.1, 137.5, 133.2, 133.0, 131.8, 126.3, 125.0, 124.5, 123.1, 121.9, 121.7, 121.7, 121.2, 121.0, 115.3, 110.9, 110.0, 49.4 (CH_2, NCH_2CO) ppm; anal. calcd for $C_{23}H_{16}BrN_3OS$: C, 59.75; H, 3.49; N, 9.09; found: C, 59.91; H, 3.63; N, 9.24.

4.2.4.13. 2-(3-(Benzo[d]thiazol-2-yl)-1H-indol-1-yl)-N-(o-tolyl) acetamide ***9m.*** White solid; yield: 74%; mp: 148–150 °C; IR (KBr, ν_{max}): 3316 (NH), 3025 (CH aromatic), 2955 (CH aliphatic), 1669 (C═O) cm^{-1}; ^1H NMR (600 MHz, DMSO-d_6) δ 9.81 (s, 1H, CONH), 8.44–8.40 (m, 1H), 8.37 (s, 1H, H-2 indole), 8.06 (d, J = 7.9 Hz, 1H), 7.98 (d, J = 8.1 Hz, 1H), 7.60 (d, J = 7.7 Hz, 1H), 7.49 (t, J = 7.7 Hz, 1H), 7.43 (d, J = 8.0 Hz, 1H), 7.40–7.30 (m, 3H), 7.23 (d, J = 7.5 Hz, 1H), 7.16 (t, J = 7.6 Hz, 1H), 7.09 (t, J = 7.4 Hz, 1H), 5.26 (s, 2H, NCH_2CO), 2.25 (s, 3H, CH_3) ppm; ^{13}C NMR (151 MHz, DMSO-d_6) δ 165.9 C═O, 162.5 (C-3a benzo[*d*]thiazole), 153.8 (C-2 benzo[*d*]thiazole), 137.4, 135.8, 133.3, 133.1, 131.8, 130.5, 126.4, 126.2, 125.6, 125.1, 124.9, 124.5, 123.1, 121.9, 121.8, 121.7, 121.1, 110.8, 110.0, 49.3 (CH_2, NCH_2CO), 17.9 (CH_3) ppm; anal. calcd for $C_{24}H_{19}N_3OS$: C, 72.52; H, 4.82; N, 10.57; found: C, 72.67; H, 4.99; N, 10.71.

4.2.4.14. 2-(3-(Benzo[d]thiazol-2-yl)-1H-indol-1-yl)-N-(4-ethyl-phenyl)acetamide ***9n.*** White solid; yield: 74%; mp: 156–158 °C; IR (KBr, ν_{max}): 3321 (NH), 3065 (CH aromatic), 2930 (CH aliphatic), 1673 (C═O) cm^{-1}; ^1H NMR (600 MHz, DMSO-d_6) δ 10.41 (s, 1H, CONH), 8.43–8.41 (m, 1H), 8.36 (s, 1H, H-2 indole), 8.07 (d, J = 7.5 Hz, 1H), 7.99 (d, J = 8.0 Hz, 1H), 7.58–7.54 (m, 1H), 7.53–7.47 (m, 3H), 7.38 (ddd, J = 8.2, 7.2, 1.2 Hz, 1H), 7.33–7.30 (m, 2H), 7.16 (d, J = 8.4 Hz, 2H), 5.20 (s, 2H, NCH_2CO), 2.55 (q, J = 7.6 Hz, 2H, Ph-CH_2), 1.15 (t, J = 7.6 Hz, 3H, CH_3) ppm; ^{13}C NMR (151 MHz, DMSO-d_6) δ 165.4 C═O, 162.4 (C-3a benzo[*d*]thiazole), 153.7 (C-2 benzo[*d*]thiazole), 139.0, 137.4, 136.3, 133.2, 133.0, 128.1, 126.2, 124.9, 124.4, 123.0, 121.8, 121.7, 121.6, 121.0, 119.3, 110.8, 109.9, 49.4 (CH_2, NCH_2CO), 27.6 (Ph-CH_2), 15.7 (CH_3) ppm; anal. calcd for $C_{25}H_{21}N_3OS$: C, 72.97; H, 5.14; N, 10.21; found: C, 73.11; H, 5.29; N, 10.36.

4.3. MTT assay

Three cancer cell lines including (A549, SW480, and HepG2) and a normal cell line (MRC-5) were included. All cell lines were attained from the National Cell Bank of Iran (NCBI, Pasteur Institute, Tehran, Iran). A549 and SW480 cells were cultured in RPMI-1640 medium, while HepG2 and MRC-5 cells were cultured in DMEM high glucose (HG) with 10% fetal bovine serum (FBS) (Gibco Invitrogen Co., Scotland, UK) and supplemented with antibiotics (penicillin and streptomycin, 10% v/v). The cells were cultured at 37 °C in a humid atmosphere containing 5% CO_2. All the synthesized compounds (**9a–n**) were evaluated by the standard 3-(4,5-dimethylthiazol-yl)-2,5-diphenyl-tetrazolium bromide (MTT) assay as described previously. The cells were harvested using trypsin/EDTA 0.5% solution and then seeded in 96-well microplates at a density equal to 1×10^4 per 100 μL of complete culture medium. After incubation for 24 h, the cells were exposed with different concentrations of cisplatin (as the positive control) and the synthesized derivatives (1–500 μM). After 72 h of incubation, the media was changed with the fresh MTT solution. Then, the plates were incubated for 4 h at 37 °C, the media was removed, DMSO was added, and the cells were incubated at 37 °C for another 10 min in the dark. Finally, the absorbance of each well was measured at 490 nm by an ELISA microplate reader. Data analysis was done using Excel 2016 and GraphPad Prism 5. The results were stated as mean IC_{50} values ± SD.[32–34]

4.4. Cell cycle

The total number of 5×10^4 A549 cells were seeded into 24-well plates and cultured under standard conditions for 16 h. After treatment of cells with 7.9 μM (IC_{50}) of **9d** for 48 h, cells were harvested with 0.25% trypsin, followed by washing with PBS and stained with PI (5 μL, 1 mg mL^{-1}), and 1U of RNase A. Cell cycle analysis was performed using flow cytometry (BD FACSCalibur Flow Cytometer, BD, USA). The DNA content was analyzed using Flowjo 10.0 software.[35]

4.5. Apoptosis assay

A total number of 1×10^5 A549 cells were pre-cultured for 16 h in 24 well plates. After exposure to 7.9 μM (IC_{50}) of **9d** for 48 h, Annexin V-FITC/PI staining was performed using eBioscience™ Annexin V apoptosis detection kit (Invitrogen). Cells were washed with phosphate-buffered saline (PBS) and 1000 μL 1× binding buffer. Then, the cells were suspended in 100 μL of binding buffer containing 5 μL of Annexin V-FITC for 15 min. After staining, the cells were washed again and resuspended in 200 μL of the binding buffer containing 5 μL of PI solution. Apoptotic cell populations were quantified using BD FACS Calibur™ flow cytometry (BD Biosciences, San Jose, CA, USA).[36,37]

4.6. Prediction of drug-likeness, pharmacokinetic and toxicity properties

Drug-likeness profiling was predicted by the SwissADME (https://www.swissadme.ch) free web tool. The *in-silico* predictions of pharmacokinetic and toxicity properties were carried out using preADMET (https://preadmet.qsarhub.com).

4.7. Molecular docking

The molecular docking study was conducted using AutoDock 4.2 software. The 3D crystal structure of EGFR in complex with erlotinib (PDB code: 1M17) was downloaded from the protein data bank. Before docking water molecules and erlotinib were removed from the protein structure, and Gasteiger charges and polar hydrogens were added. The self-dock was performed to confirm the validity of the docking procedure. The energy minimization of ligands was done with CHEM 3D 16.0. The orientations and interactions were visualized with Discovery Studio 2021 Client.

Author contributions

N. M. S.: methodology, investigation. M. N.: methodology, investigation. N. D.: data curation. Z. D.: investigation, writing.

M. E.: formal analysis. S. S.: validation. Y. G.: conceptualization, resources. S. N. G.: formal analysis. A. G.: data curation. M. R. M.-T.: resources, methodology. B. L.: data curation, validation. M. M.: methodology, conceptualization, supervision, project administration, editing. S. R.: conceptualization, supervision, project administration methodology, editing and writing.

Conflicts of interest

The authors declare no conflict of interest.

Data availability

The data supporting this article have been included in the supplementary information (SI). Supplementary information: ^{1}H NMR, ^{13}C NMR spectra. See DOI: https://doi.org/10.1039/d5ra08263c.

Acknowledgements

This work was supported by the Vice-Chancellor for Research, Shiraz University of Medical Sciences, Iran (Gant Number: 33720).

References

1 Z. Wu, F. Xia and R. Lin, *J. Hematol. Oncol.*, 2024, **17**, 119.
2 R. L. Siegel, A. N. Giaquinto and A. Jemal, *Ca-Cancer J. Clin.*, 2024, **74**, 12–49.
3 H. ur Rashid, Y. Xu, Y. Muhammad, L. Wang and J. Jiang, *Eur. J. Med. Chem.*, 2019, **161**, 205–238.
4 J. Zugazagoitia, C. Guedes, S. Ponce, I. Ferrer, S. Molina-Pinelo and L. Paz-Ares, *Clin. Ther.*, 2016, **38**, 1551–1566.
5 T. Qadir, A. Amin, P. K. Sharma, I. Jeelani and H. Abe, *Open J. Med. Chem.*, 2022, **16**, e187410452202280.
6 A. Gomtsyan, *Chem. Heterocycl. Compd.*, 2012, **48**, 7–10.
7 A. Irfan, F. Batool, S. A. Zahra Naqvi, A. Islam, S. M. Osman, A. Nocentini, S. A. Alissa and C. T. Supuran, *J. Enzyme Inhib. Med. Chem.*, 2020, **35**, 265–279.
8 I. Aayishamma, G. S. P. Matada, R. Pal, A. Ghara, N. V. S. S. Aishwarya, B. Kumaraswamy, K. R. Hosamani and B. Manjushree, *Eur. J. Med. Chem.*, 2024, 116831.
9 D.-F. Shi, T. D. Bradshaw, S. Wrigley, C. J. McCall, P. Lelieveld, I. Fichtner and M. F. Stevens, *J. Med. Chem.*, 1996, **39**, 3375–3384.
10 A. Blyufer, S. Lhamo, C. Tam, I. Tariq, T. Thavornwatanayong and S. S. Mahajan, *Int. J. Oncol.*, 2021, **59**, 1–11.
11 M. K. Lemieszek, A. Stepulak, K. Sawa-Wejksza, A. Czerwonka, C. Ikonomidou and W. Rzeski, *Anti-Cancer Agents Med. Chem.*, 2018, **18**, 565–572.
12 S. M. Hassan, A. Farid, S. S. Panda, M. S. Bekheit, H. Dinkins, W. Fayad and A. S. Girgis, *Pharmaceuticals*, 2024, **17**, 922.
13 T. Sravanthi and S. Manju, *Eur. J. Pharm. Sci.*, 2016, **91**, 1–10.
14 A. Vinod, H. M. Chandra Mouli, A. Jana and R. Peraman, *Med. Chem. Res.*, 2024, **33**, 1100–1132.
15 I. Ali, M. N. Lone, Z. A. Al-Othman, A. Al-Warthan and M. M. Sanagi, *Curr. Drug Targets*, 2015, **16**, 711–734.
16 M. A. Jordan, R. H. Himes and L. Wilson, *Cancer Res.*, 1985, **45**, 2741–2747.
17 T. Verma, A. Mehra and A. Mittal, *Chem. Biodiversity*, 2026, **23**, e02968.
18 H. Ito, T. Kanzawa, S. Kondo and Y. Kondo, *Int. J. Oncol.*, 2005, **26**, 589–596.
19 A. Sakr, S. Rezq, S. M. Ibrahim, E. Soliman, M. M. Baraka, D. G. Romero and H. Kothayer, *J. Enzyme Inhib. Med. Chem.*, 2021, **36**, 1810–1828.
20 S. Puri, K. Stefan, S. L. Khan, J. Pahnke, S. M. Stefan and K. Juvale, *J. Med. Chem.*, 2022, **66**, 657–676.
21 K. S. Prasad, R. R. Pillai, M. P. Ghimire, R. Ray, M. Richter, C. Shivamallu, A. S. Jain, S. K. Prasad, S. Armaković and S. J. Armaković, *J. Mol. Struct.*, 2020, **1217**, 128445.
22 F. Doganc, T. Ozkan, N. Farhangzad, A. Mavideniz, I. Celik, A. Sunguroglu and H. Göker, *Bioorg. Chem.*, 2024, **148**, 107429.
23 E. R. El-Sawy, H. M. Abo-Salem, K. Mahmoud, E. S. Zarie, A. M. El-Metwally and A. H. Mandour, *Int. J. Pharm. Pharm. Sci.*, 2015, 377–385.
24 C. A. Lipinski, *Drug Discovery Today:Technol.*, 2004, **1**, 337–341.
25 S. Ranjbar, O. Firuzi, N. Edraki, O. Shahraki, L. Saso, M. Khoshneviszadeh and R. Miri, *MedChemComm*, 2017, **8**, 1919–1933.
26 S. Ranjbar, F. F. Lashkarian, M. Khoshneviszadeh, F. Moosavi, A. Sakhteman, F. Zargari, L. Saso, O. Firuzi and N. Edraki, *J. Mol. Struct.*, 2023, **1285**, 135427.
27 S. Ranjbar, R. Khonkarn, A. Moreno, H. Baubichon-Cortay, R. Miri, M. Khoshneviszadeh, L. Saso, N. Edraki, P. Falson and O. Firuzi, *Toxicol. Appl. Pharmacol.*, 2019, **362**, 136–149.
28 G. S. Kapoor, A. Christie and D. M. O'Rourke, *Cancer Biol. Ther.*, 2007, **6**, 571–579.
29 S. Sigismund, D. Avanzato and L. Lanzetti, *Mol. Oncol.*, 2018, **12**, 3–20.
30 W. A. Zagha, G. H. Elgemeie, R. A. Azzam, S. A. Aljuhr and T. M. Sakr, *Curr. Pharm. Des.*, 2025, 2559–2593.
31 E. A. Abd El-Meguid, A. M. Naglah, G. O. Moustafa, H. M. Awad and A. M. El Kerdawy, *Bioorg. Med. Chem. Lett.*, 2022, **58**, 128529.
32 M. Khoshneviszadeh, O. Firuzi, M. Aminsafaee, M. Kashefizadeh, S. Ranjbar, Z. Rezaei, H. Sadeghpour, F. Zargari, R. Miri and N. Edraki, *Iran. J. Pharm. Res.*, 2021, **20**, 161.
33 S. Ranjbar, P. Sadeghian, S. Khademian, M. Emami, Z. P. Jahromi, S. H. Mirmajidi, F. Zare, M. Negahdaripour, Y. Ghasemi and M. Khoshneviszadeh, *Heliyon*, 2024, **10**, e29850.
34 S. Ranjbar, M. R. Shabanpoor, Z. Dehghani, O. Firuzi, N. Edraki and M. Khoshneviszadeh, *Braz. J. Pharm. Sci.*, 2021, **57**, e18074.
35 S. Ranjbar, M. Khoshneviszadeh, M. Tavakkoli, R. Miri, N. Edraki and O. Firuzi, *Mol. Diversity*, 2022, 1–20.

36 N. Dastyafteh, M. Negahdaripour, M. H. Sayahi, M. Emami, Y. Ghasemi, E. Safaei, H. Azizian, Z. P. Jahromi, M. Asadi and M. R. Mohajeri-Tehrani, *RSC Adv.*, 2024, **14**, 35323–35335.

37 A. S. S. Asl, S. Ranjbar, M. H. Sayahi, Z. Dehghani, A. M. Taherkhani, M. Negahdaripour, N. Dastyafteh, M. Emami, S. Safapoor and A. Ghahramani, *RSC Adv.*, 2025, **15**, 37447–37460.